Atmos. Chem. Phys. Discuss., 14, 4457–4503, 2014
www.atmos-chem-phys-discuss.net/14/4457/2014/
doi:10.5194/acpd-14-4457-2014
© Author(s) 2014. CC Attribution 3.0 License.

Atmospheric Chemistry and Physics Discussions
Open Access

This discussion paper is/has been under review for the journal Atmospheric Chemistry and Physics (ACP). Please refer to the corresponding final paper in ACP if available.

The added value of water isotopic measurements for understanding model biases in simulating the water cycle over Western Siberia

V. Gryazin[1,2], C. Risi[3], J. Jouzel[1], N. Kurita[4], J. Worden[5], C. Frankenberg[5], V. Bastrikov[1,2,6], K. Gribanov[2], and O. Stukova[2]

[1]Laboratoire des Sciences du Climat et de l'Environnement, Gif-sur-Yvette, France
[2]Institute of Natural Science, Ural Federal University, Ekaterinburg, Russia
[3]Laboratoire de Météorologie Dynamique, Paris, France
[4]Japan Agency for Marine-Earth Science and Technology, Yokosuka, Japan
[5]Jet Propulsion Laboratory, California Institute of Technology, Pasadena, California, USA
[6]Institute of Industrial Ecology UB RAS, Ekaterinburg, Russia

Received: 14 December 2013 – Accepted: 5 February 2014 – Published: 20 February 2014

Correspondence to: V. Gryazin (gryazin.victor@mail.ru)

Published by Copernicus Publications on behalf of the European Geosciences Union.

Abstract

We evaluate the isotopic composition of water vapor and precipitation simulated by the LMDZ GCM over Siberia using several datasets: TES and GOSAT satellite observations of tropospheric water vapor, GNIP and SNIP precipitation networks, and daily, in-situ measurements of water vapor and precipitation at the Kourovka site in Western Siberia. We use δD vs. humidity diagrams to explore the complementarity of these two variables to interpret model biases in terms of the representation of processes. LMDZ captures the spatial, seasonal and daily variations reasonably well. It systematically overestimates δD in the vapor and precipitation, a bias that is most likely associated with a misrepresentation of air mass origin.

The performance of LMDZ is put in the context of other isotopic models from the SWING2 models. There is significant spread among models in the simulation of δD, and of the δD vs. humidity relationship. This confirms that δD brings additional information compared to humidity only. We specifically investigate the added value of water isotopic measurements to interpret the warm and dry bias feature by most GCMs over mid and high latitude continents in summer. LMDZ simulates the strongest dry bias on days when it simulates the strongest enriched bias in δD. The analysis of the slopes in δD vs. humidity diagrams and of processes controlling δD and humidity variations suggests that the cause of the moist bias could be either a problem in the large-scale advection transporting too much dry and warm air from the south, or insufficient surface evaporation.

1 Introduction

General circulation models (GCMs) have persistent and systematic biases in the representation of modern climate and its associated water cycle (Meehl et al., 2007). One example of these biases is the systematic warm and dry bias over mid latitude continental regions in summer, which is evident especially in the Great Plains of the United

ACPD
14, 4457–4503, 2014

CC BY

States and in Central and Eastern (Cattiaux et al., 2013; Kittel et al., 1997). This bias may reflect a misrepresentation of the water cycle, land-surface feedbacks (Bellprat et al., 2013; Moberg and Jones, 2004), or cloud feedbacks (Boé, 2013; Cattiaux et al., 2013). This misrepresentation causes some doubts on the climate projections simulated for these regions. In particular, there is evidence for a link between the dry and warm bias in mid-latitude continents in summer for present-day and future projections of evapotranspiration (Boé and Terray, 2008) and temperature extremes (Boberg and Christensen, 2012; Christensen and Boberg, 2012). Credible climate projections thus require a correct simulation of the present-day climate, water cycle, and associated processes.

Several approaches have been proposed to investigate the persistent warm and dry bias over mid-latitude continents in summer. Sensitivity tests to the model physics have shown that biases can be reduced by improving parameterizations or tuning parameters related to the representation of soil processes (Cheruy et al., 2013; Polcher et al., 1996). Experiments performed running GCMs in forecast mode with a realistic initialization of meteorological variables have also suggested that the bias is associated with land-surface interactions (Klein et al., 2006). Here, we show that comparing the simulated water stable isotopic composition of water vapor to measurements can help us diagnose the source of model biases over continental regions in summer.

The water molecule has several isotopologues. The most common isotopologue is $H_2^{16}O$ (hereafter called H_2O), but heavier isotopologues are also found: $HD^{16}O$ (hereafter called HDO, with D standing for deuterium) and $H_2^{18}O$. The water vapor isotopic composition (e.g., the concentration in HDO and $H_2^{18}O$ with respect to H_2O) is affected during phase changes and conserved during transport. Therefore, the water vapor composition records the various evaporation and condensation processes undergone within an air parcel throughout its history. For example, oceanic evaporation and continental evapotranspiration leave different imprints on the water vapor composition (Gat and Matsui, 1991; Risi et al., 2013; Salati et al., 1979; Simonin et al., 2013). Water vapor and subsequent precipitation is further affected by large-scale circulation

ACPD
14, 4457–4503, 2014

(Frankenberg et al., 2009; Galewsky and Hurley, 2010) and convective and cloud processes (Bony et al., 2008; Galewsky and Hurley, 2010; Risi et al., 2008; Yoshimura et al., 2010). In turn, water vapor isotopic measurements can help diagnose biases in the way models simulate the water cycle. For example, isotopic measurements have been used to understand systematic biases in the precipitation frequency in the tropics (Lee et al., 2009) and in subtropical tropospheric humidity (Risi et al., 2012a, b). If biases in evapotranspiration, in large-scale moisture transport or in cloud processes contribute to the dry and warm model biases over continental regions in summer, then water isotopic measurements may help diagnose them.

Before we can operationally use water isotopic measurements to diagnose causes of model biases, the first step is to understand what controls the water isotopic composition. In this paper, we focus on this first step, and give insight on how water isotopic measurements could be used for model evaluation. With this aim, we exploit a new set of continuous isotopic measurements in low-level atmospheric water vapor and precipitation at Kourovka (70 km north-west from Ekaterinburg) near the western boundary of Western Siberia. This dataset is complemented by satellite measurements (Frankenberg et al., 2013; Worden et al., 2007) and compared with existing isotopic GCMs. In particular, using the LMDZ GCM (Risi et al., 2010b), processes controlling water isotopic composition are investigated and sources of model-data mismatches are discussed.

In Sect. 2, datasets and models are described. In Sect. 3, the LMDZ GCM is evaluated against satellite and precipitation networks data and its performance is put in a broader context through comparison with other GCMs. The ability of LMDZ to represent the water cycle is evaluated in Sect. 4 using continuous measurements of water isotopic composition in Kourovka. In Sect. 5, physical processes controlling water vapor and precipitation composition are investigated. We discuss the results and conclude in Sect. 6.

ACPD
14, 4457–4503, 2014

2 Data and methods

2.1 Isotopic definitions

Isotope ratios are commonly reported relative to a standard in δ-notation (Craig, 1961):

$$\delta = (R_{\text{sample}}/R_{\text{standart}} - 1) \cdot 1000(‰),$$

where the standard used is Vienna Standard Mean Ocean Water (VSMOW), δ represent either δD or δ^{18}O, and R is the relative composition of HDO or $H_2^{18}O$ compared to H_2O.

Deuterium-excess is defined with respect to the Global Meteoric Water Line (GMWL, $\delta D = 8 \cdot \delta^{18}O + 10‰$) (Dansgaard, 1964):

$$\text{d-excess} = \delta D - 8 \cdot \delta^{18}O(‰).$$

Values that fall on the GMWL have a d-excess of 10 ‰ by definition. Since equilibrium Rayleigh condensation processes roughly follow the GMWL slope of 8, deviations in d-excess can provide information about the environmental conditions during non-equilibrium processes.

2.2 LMDZ model and simulations

The dynamical equations of the GCM LMDZ are discretized in a latitude-longitude grid, with a resolution of $2.5^\circ \times 3.75^\circ$ and 39 vertical levels. The physical package is described in detail by (Hourdin et al., 2006). Each grid cell is divided into four subsurfaces: ocean, land, ice sheet and sea ice. The land surface is represented as a simple bucket model, and land surface evaporation is calculated as a single flux: no distinction is made between transpiration, bare soil evaporation, or evaporation of intercepted water by the canopy.

To ensure a realistic large-scale circulation and daily variability (Risi et al., 2010b; Yoshimura et al., 2008), horizontal winds at each vertical level are nudged by ECMWF reanalyses (Uppala et al., 2005).

ACPD
14, 4457–4503, 2014

Isotopologues of water ($H_2^{16}O$, $H_2^{18}O$ and HDO) are transported and passively mixed by the large-scale advection and various air mass fluxes. Due to simplicity of the land surface parameterization in LMDZ4, no information is available about the fraction of the evapotranspiration flux arising from fractionating evaporation. From the other hand, the model takes into account the evolution of the compositions of both the rain and the surrounding vapor as the rain drops reevaporate (Bony et al., 2008). The isotope-enabled version of the GCM LMDZ is described in detail by Risi et al. (2010b).

2.3 SWING2 models and simulations

To put LMDZ results into a broader context, we compare with other isotopic GCM simulations archived in the SWING2 (Stable Water INtercomparison Group phase 2) database (http://people.su.se/~cstur/SWING2). We use nine simulations from seven models (LMDZ4, ECHAM, CAM2, GISS modelE, isoGSM, HadAM and MIROC). Some simulations were nudged by reanalyses and other were not. More details about these SWING2 simulations can be found in Risi et al. (2012a).

2.4 In-situ dataset at Kourovka

The measurements of atmospheric surface water vapor isotopic composition are performed by the Picarro isotopic analyzer L2130-i based on wavelength-scanned cavity ring down spectroscopy (WS-CRDS). This instrument was installed in the Kourovka astronomical observatory (57.037° N, 59.547° E, 300 m a.s.l.) and has provided continuous measurements of δD and δ^{18}O since April 2012. The observatory is located 70 km north-west of Ekaterinburg in a forest region. Air is sampled at 8 m height.

The instrumental uncertainty is conservatively estimated to be 1.4 ‰ for δD and 0.23 ‰ for δ^{18}O, respectively (Steen-Larsen et al., 2013). However, at low humidity levels (< 1500 ppmv) the instrument reveals a strong increase in uncertainty estimated to be 5.6 ‰ for δD and 0.92 ‰ for δ^{18}O at 1000–1500 ppmv and 11.2 ‰ for δD and 1.84 ‰ for δ^{18}O at 500–1000 ppmv (Bastrikov et al., 2014). The measurements below

ACPD
14, 4457–4503, 2014

500 ppmv are considered to be beyond the instrument measuring capabilities and are not used in the analysis.

From June 2012 until September 2012, the Picarro calibration system was not working properly due to a leakage. For this reason, the data obtained during this period are associated with a reduced accuracy. We decided to limit the use of these data to δD measurements only, for which this higher uncertainty is acceptable. After the replacement of the faulty elements on 18 September 2012, the instrument has revealed good stability and reliability. A detailed overview of the WS-CRDS measurement system setup, calibration, and maintenance can be found in Bastrikov et al. (2014).

In addition to the measurements described above, precipitation samples have been collected at Kourovka since the end of October 2012. Measurements were performed on the Picarro isotopic analyzer L2130-i installed at the Ural Federal University (Ekaterinburg), which is equipped with a liquid water analysis system. Instrumental precision is 1.0 ‰ for δD and 0.1 ‰ for δ^{18}O.

2.5 Precipitation networks

To put the Kourovka measurements into a broader regional context and to evaluate the capacity of LMDZ to capture the spatial and seasonal patterns of precipitation isotopic composition, we combine two networks: GNIP (Global Network for Isotopes in Precipitation) (Rozanski et al., 1993) and SNIP (Siberian Network for Isotopes in Precipitation) (Kurita et al., 2004). Both δ^{18}O and δD are measured in the rain samples, allowing the calculation of the d-excess.

2.6 Satellite datasets

To evaluate the spatial and seasonal patterns of vapor isotopic composition, we use two satellite datasets measuring tropospheric δD. At present, satellite measurements cannot provide δ^{18}O with sufficient precision for d-excess calculations to be useful for scientific applications. GOSAT measurements enable the retrieval of the total-column

ACPD
14, 4457–4503, 2014

water vapor content in both H_2O and HDO (Frankenberg et al., 2013). Since most of the total-column vapor is in the lower troposphere, column-integrated δD is mainly sensitive to the δD of the boundary layer. TES measurements enable the retrieval of some information on the vertical distribution of specific humidity and δD in the troposphere (Worden et al., 2006, 2007). Recent processing of the data leads to enhanced sensitivity in northern latitudes and to a higher degree of freedom of the signal (Worden et al., 2012). For clear sky scenes these data can distinguish air-parcels at 900 hPa from those at 400 hPa. A correction was applied on observed δD following the calibration study of Worden et al. (2011). More details on the GOSAT and TES data used and the quality selection criteria can be found in Risi et al. (2013).

In order to rigorously compare LMDZ with GOSAT or TES, we take into account spatio-temporal sampling and we apply averaging kernels to the model outputs to account for the vertical resolution and use of a priori constraints of the satellite retrievals. More details on the model-data comparison methodology are in Risi et al. (2012a) and Risi et al. (2013). We focus only on comparing spatial and temporal variations in order to minimize uncertainties related to biases in the satellite data (Frankenberg et al., 2013; Worden et al., 2011).

2.7 δD vs. humidity diagrams

2.7.1 Theoretical curves in δD vs. humidity diagrams

To a first order, in mid and high latitudes, δD follows Rayleigh distillation (Dansgaard, 1964):

$$\ln(R_v) = \ln\left(R_{v_0}\right) - (\alpha - 1)\cdot\ln(q_0) + (\alpha - 1)\cdot\ln(q) \sim \delta D/1000, \quad (1)$$

where R_v is the isotopic ratio in the final vapor, R_{v_0} and q_0 are the initial isotopic ratio and specific humidity, respectively, and α is the fractionation coefficient.

Therefore, to first order, δD correlates with specific humidity q (Schneider et al., 2010). When investigating what we can learn from water isotopic measurements, we

ACPD
14, 4457–4503, 2014

need to investigate the added value compared to q. A way to investigate this is to analyze the relationship of δD as a function of q (Worden et al., 2007). For even better consistency with a Rayleigh distillation, we can also analyze the relationship of δD as a function of ln(q), in which the Rayleigh distillation is approximately a straight line. Figure 1 shows how different processes may affect the relationship of δD as a function of ln(q). An air mass that cools and loses water vapor by condensation follows the Rayleigh distillation line (red). Mixing between air masses that have undergone different degrees of distillation follows a hyperbolic shape with more enriched values for a given q (green) (Galewsky and Hurley, 2010). Recycling of precipitation, either through local transpiration of soil water or through re-evaporation of falling raindrops follows mixing lines with more depleted values for a given q (blue).

Such plots can be instructive qualitatively. They may however be difficult to apply quantitatively to the data due to various factors affecting these curves. For example, the Rayleigh distillation line is sensitive to δD in the initial vapor, which may depend on the existence of convective activity (Jouzel and Koster, 1996; Lawrence et al., 2004). The mixing lines are very sensitive to the $q - \delta$D properties of the end members (compare the different green lines on Fig. 1). Re-evaporation lines are sensitive evaporation conditions (compare the different pink lines on Fig. 1).

2.7.2 Consequences for the interpretation of model-data differences in δD

Model-data differences in δD ($\Delta\delta$D) can be interpreted in the light of δD-vs-q diagrams: if δD is misrepresented, it could be either because q is misrepresented, or because the δD-vs-q relationship is misrepresented. For example, if δD is controlled by Rayleigh distillation and LMDZ misrepresents the intensity of this distillation, then LMDZ will overestimate both q and δD. On days when LMDZ overestimates q the most, LMDZ will overestimate δD the most. In addition, the slope of the $\Delta\delta$D vs. Δ ln(q) would be the same as that of δD vs. ln(q): indeed, based on Eq. (1), $\Delta\delta$D relates to

ACPD
14, 4457–4503, 2014

Δq following:

$$\Delta \ln(R_v) = (\alpha - 1) \cdot \Delta \ln(q).$$

Similarly, if δD is controlled by mixing and if LMDZ misrepresents the proportion of this mixing, it can be shown that LMDZ will overestimate δD the most on days when it overestimates q the most and that the slope of the $\Delta\delta$D vs. $\Delta \ln(q)$ would also be similar to that of δD vs. $\ln(q)$.

In contrast, if LMDZ misrepresents the initial δD of water vapor, there will be a systematic offset between the data and the model δD, and no particular relationship is expected between $\Delta\delta$D and $\Delta \ln(q)$.

3 Model evaluation of spatial and seasonal variations

To evaluate the spatial and seasonal variations over Siberia simulated by LMDZ, we use satellite and precipitation network data.

3.1 Spatial variations

Figure 2 shows the maps of annual mean water vapor δD and precipitation δ^{18}O, and d-excess. For satellite data, we subtract domain average values to focus on spatio-temporal variations independently of possible systematic biases in the data. Both GOSAT and TES data exhibit the temperature effect, with δD decreasing with latitude, and the continental effect, with δD decreasing along trajectories from west to east (Fig. 2a and c). These effects are also visible in the precipitation δD (Fig. 2e). To first order, LMDZ captures these patterns qualitatively well (Fig. 2b, d and f). For d-excess, the scarcity of data makes it difficult to extract any clear spatial signal. However, most of the data features are decreasing d-excess trend poleward and eastward (Fig. 2g). LMDZ captures this pattern qualitatively well (Fig. 2h).

ACPD
14, 4457–4503, 2014

For a more quantitative evaluation Figs. 3 and 4 show north-south and west-east transects around Kourovka. The poleward depletion associated with the temperature effect can clearly be seen in GOSAT, TES, and precipitation networks datasets (Fig. 3a–c). Compared to both satellite datasets, LMDZ underestimates the latitudinal gradient of δD (Fig. 3a and b), a bias that was already noticed by Risi et al. (2012a). We investigated the latitudinal gradients at different altitudes using the TES data, which has some vertical information. LMDZ underestimates the latitudinal gradient from the surface to 800 hPa, and slightly overestimates it from 800 to 550 hPa. Above 550 hPa, the TES sensitivity to δD becomes too low to conclude. Therefore, the underestimate of the latitudinal gradient originates from the boundary layer. For example, it could be due to a wrong representation of the latitudinal variations in evapo-transpiration, with too much evapo-transpiration in the northern part of Siberia, or too little evapo-transpiration in the southern part. A seasonal analysis of the latitudinal gradients shows that the latitudinal gradient is underestimated only in summer. This is consistent with the hypothesis of a mis-representation of evapo-transpiration, since evapo-transpiration occurs mainly in summer.

For the precipitation, the data is noisier due to the scarcity of observations. We cannot detect any obvious bias in the simulation of the latitudinal gradient of δD compared to the data (Fig. 3c).

For d-excess, the data is much noisier, but the decreasing trend with latitude can be observed. This could be associated with the Rayleigh distillation, which first decreases d-excess until about $-20\,^{\circ}$C and increases it below (Masson-Delmotte et al., 2008). LMDZ captures this d-excess trend.

The eastward depletion associated with the continental effect is very well captured by LMDZ compared to GOSAT, TES, and precipitation networks datasets (Fig. 4a–c). If the continental effect is modulated by continental recycling (Kurita et al., 2004), then this suggest that LMDZ represents the East-West continental recycling gradient satisfactorily. No clear eastward trend can be noticed in observed d-excess. Simulated d-excess is less noisy than in observations but the large noise and lack of clear signal

ACPD
14, 4457–4503, 2014

in the data makes it difficult to assess whether the model is consistent or not with the data.

The ECHAM model was compared to the same satellite datasets and also showed a good capacity for simulating the observed spatial variations (Butzin et al., 2013).

3.2 Seasonal variations

As is common in most of the Northern Hemisphere, δD is more enriched in summer and more depleted in winter (Fig. 5a–c), consistent with the temperature effect. LMDZ captures this seasonality qualitatively well, though δD variations are underestimated compared to both satellite datasets (Fig. 5a and b). It also seems that the LMDZ seasonal cycle is delayed by a few weeks. These problems do not appear in the precipitation networks. Both TES and GOSAT have fewer usable data points in the winter. It is possible that there are too few samples to make a robust comparison. The precipitation networks show large spatial noise for d-excess (Fig. 5d); however the comparison suggests that LMDZ misrepresents the seasonal cycle of d-excess.

3.3 Possible causes of model-data differences

We note that LMDZ underestimates both the latitudinal and the seasonal variations of isotopic composition. A common bias of GOSAT and TES towards overestimating δD variations is unlikely given that they used independent wavelengths and retrieval algorithms.

If the underestimate of latitudinal and seasonal variations by LMDZ in the lower and mid troposphere is real, what might cause it? As explained in Sect. 2.7, the underestimate of δD variations may be associated either with an underestimate of q variations or with an underestimate of the slope of δD as a function of q. Figure 6 shows that for both latitudinal and seasonal variations, the range of simulated q variations are comparable with observations, but the slope of δD vs. q is weaker in the LMDZ results. Therefore, the δD discrepancies are not due to temperature or q variations, but rather

ACPD
14, 4457–4503, 2014

to the type of hydrological processes (condensation, mixing or re-evaporation). For example, there could be too much diffusion in the advection scheme (Risi et al., 2012a, b) or an over-estimate of continental recycling (Risi et al., 2013).

3.4 Comparison with other models

To put the LMDZ results into a broader context, we compare them with those of other model simulations from the SWING2 archive (Fig. 7). Since daily outputs are not available, we cannot collocate the model outputs with the satellite datasets and we cannot convolve them with the appropriate averaging kernels. Therefore, in this section, we just compare the climatological averages of the different models with each other, without any comparison with TES or with GOSAT. SWING2 simulations exhibit a large spread in their representation of the latitudinal gradient in the mid troposphere (Fig. 7a), with gradients ranging from 1.1 ‰ degree^{-1} to 2.5 ‰ degree^{-1}. Compared to the other models, LMDZ does not simulate the weakest gradient, suggesting that these other models might share the same tendency to underestimate this gradient compared to the data. A comparable spread remains in the lower troposphere (not shown).

What might cause this spread? First, some of this spread is related to the simulated q, which reflects the basic climatology. For example, the steepest latitudinal gradient in δD is featured by the free (i.e. not nudged) simulation of LMDZ, which is associated to the largest range of q along the latitudinal gradient (Fig. 7b). The weakest latitudinal gradient in δD is featured by the CAM2 model, which is associated to the smallest range of q along the latitudinal gradient. Both models have a similar δD-vs-q slope, however (Fig. 7b). Second, some of the spread is related to the δD-vs-q slope, which reflects more subtle physical processes. For example, one of the steepest latitudinal gradients in δD is featured by the HadAM model, which is associated with the steepest δD-vs-q slope (Fig. 7b). The reverse is true for isoGSM.

SWING2 simulations also exhibit a large spread in their representation of the seasonal cycle of δD at Kourovka, with seasonal magnitudes ranging from 40 to 160 ‰ (Fig. 7c). Again, LMDZ does not simulate the weakest seasonality among the models,

ACPD
14, 4457–4503, 2014

suggesting that other models might share this same tendency. There is no relationship between the seasonality in δD and in q. This shows that the seasonality in δD reflects some physical processes that are not immediately detectable when looking at conventional variables, thus supporting the added value of water isotopic measurements to better evaluate these processes (Risi et al., 2012a, b).

4 Evaluation over Kourovka

4.1 Timeseries for water vapor

Continuous measurements of water vapor isotopic composition from Kourovka with the Picarro instrument have allowed us to analyze daily timeseries from April until the end of 2012. Comparison of observations with the results of LMDZ-iso simulation of water vapor for 2012 at Kourovka is shown on Fig. 8. The LMDZ results correlate very well with the observations for the whole period of measurement and show values greater than 0.94 for both isotopologues (Table 1).

LMDZ underestimates specific humidity (q) most of the time and the difference between model and observations reaches a maximum ($8\,\mathrm{g\,kg^{-1}}$) in August. The daily model-data correlation for q is better in winter and rises to 0.94. This is consistent with the summer dry bias of LMDZ discussed in the introduction. A day bias was also noticed in the free troposphere compared to the IASI data (Pommier et al., 2013). Model-data differences will be interpreted in the next section.

LMDZ almost always overestimates observed δD and δ^{18}O, with the exception of December, where there is very low q. The fact that the LMDZ results are too enriched compared to observations is consistent with the fact that the LMDZ results were too enriched compared to SNIP observations (Figs. 3 and 4). Compared to both datasets, the LMDZ results are on average about 20‰ too enriched.

As previously mentioned in Sect. 2.4, it was decided not to use the data for d-excess from April to the end of September due to a leakage in the Picarro calibration system.

ACPD
14, 4457–4503, 2014

Confidence in d-excess for observations is in doubt for this period and we limit the analysis of these data to the last three months, October to December. For this period modeled d-excesses show fewer variations than observed values and remain in the range of 9 to 15 ‰. An underestimation of daily d-excess variability by GCMs had already been noticed for other mid-latitude sites (Risi et al., 2010a). Despite the large differences in values, there is a good qualitative agreement of the results in November. For example, LMDZ captures the d-excess increase in the end of October, the decrease in early November and the increase in late November.

The vapor was collected at 8 m a.g.l. In the model, the first layer is 70 m thick and the model outputs represent vapor integrated over this depth. The difference in vertical footprint could explain some mode-data discrepancy, though we expect this effect to be small. For an average δD gradient of -15 ‰ km^{-1}, the expected different between 8 m and 33 m (mean altitude of the LMDZ first level) is only 0.3 ‰.

To summarize, LMDZ captures well the temporal variations observed in ground-based measurements, especially in the winter. During the summer, the model underestimates q. All year long, it is systematically too enriched in isotopic composition.

4.2 Difference of isotopic composition between precipitation and water vapor

Figure 9 shows the daily mean difference in δD ($\delta D_p - \delta D_v$) and d-excess between precipitation and water vapor. Precipitation is snow, except during the first three days. The theoretical estimation of this difference, assuming isotopic equilibrium between precipitation and vapor, is shown as green line. Equilibrium fractionation coefficients between vapor and liquid water or ice are calculated afterwards (Majoube, 1971a, b; Merlivat and Nief, 1967). We take into account kinetic effects during snow formation, following Jouzel and Merlivat (1984).

We have found significant correlation between the model and observations for $\delta D_p - \delta D_v$ (Table 1). Observed precipitation is on average about 80 ‰ more enriched in δD than the water vapor at the surface (Fig. 9a, red dots). The LMDZ results are consistent with these observations, though there are some model-data differences for

ACPD
14, 4457–4503, 2014

individual events (Fig. 9a, blue dots). If the snow was in equilibrium with the surface water vapor, it would be about 115 ‰ more enriched (Fig. 9a, green curve). In LMDZ, the condensation occurs around 2 km on average. The condensation altitude is calculated in LMDZ as the average altitude weighted by condensation rate. The δD decreases with altitude and the vertical gradient between the surface and 2 km is about -15 ‰ km^{-1}. Therefore, most of the snow forms on average from a water vapor which is about 30 ‰ more depleted than at the surface. The fact that the observed snow is about 35 ‰ less enriched than predicted based on equilibrium with the surface water vapor is thus consistent with the fact that the snow is formed from water vapor at 2 km. In addition, daily variations in $\delta D_p - \delta D_v$ reflect variations in condensation altitude: in LMDZ, the correlation between $\delta D_p - \delta D_v$ and the condensation altitude for the entire period is -0.51.

The d-excess in observed precipitation is very similar to the d-excess in surface water vapor (Fig. 9b). LMDZ captures this property well. If the snow was in equilibrium with the surface water vapor, its d-excess would be about 5 ‰ lower. The d-excess increases with altitude and the vertical gradient between the surface and 2 km is 1 ‰ km^{-1}. Taking this effect into account, the snow d-excess should thus be around 3 ‰ lower than in the vapor. The fact that the snow and vapor from observations and simulation have a similar d-excess is currently not well understood.

In Sect. 3.1, we showed that LMDZ simulates a precipitation that is systematically too enriched. The fact that LMDZ simulates the difference between δD in precipitation and in vapor correctly confirms that the cause of the overestimation of the precipitation δD (both at Kourovka and on all GNIP and SNIP sites) is the overestimation of the δD of the vapor from which the precipitation is formed.

ACPD
14, 4457–4503, 2014

5 Processes controlling water vapor and δD

5.1 Understanding the simulated evolution in humidity and δD

5.1.1 Method for the tendency analysis

In Sect. 3.2, we showed that LMDZ reproduces well, at least qualitatively, the seasonal and daily variations in q and water vapor δD at the surface. Therefore, we can make use of LMDZ simulations to investigate in more detail the physical processes controlling these variations. The different processes affecting q and δD in the model in general are schematically illustrated in Fig. 10. Below we focus in more detail on each of them:

1. Vertical and horizontal advection by the large-scale winds (red). Since we focus on surface q and δD, only the horizontal component of the advection is non-zero. Horizontal advection may moisten or dehydrate depending on the horizontal q gradients and the direction of the wind. Similarly, it may enrich or deplete the water vapor.

2. Deep convection (green). This represents the effect of vertical motions and phase changes in convective systems. At the surface, convection dehydrates the air through subsident motions such as unsaturated downdrafts (Zipser, 1977). This subsidence also has a depleting effect on water vapor (Risi et al., 2008, 2010b). Convection may also moisten the lower levels through rain re-evaporation (Folkins and Martin, 2005). In this case, its effect on δD can be either enriching or depleting (Risi et al., 2010b; Worden et al., 2007).

3. Large-scale condensation and re-evaporation (blue). This represents the effect of phase changes occurring outside of the convective systems, such as in frontal systems or stratiform clouds. Near the surface, it may moisten the boundary layer through the evaporation of the precipitation formed by such systems or clouds. As for the evaporation of convective rain, this can either enrich or deplete the

ACPD
14, 4457–4503, 2014

water vapor. Occasionally, it may dehydrate and deplete the vapor through in-situ condensation in fogs.

4. Surface evaporation and boundary-layer processes (cyan). Unfortunately, our model diagnostics do not allow for the separation of these two effects despite their different effects on q and on δD of near-surface vapor. Surface evaporation moistens the boundary layer. Since we assume no fractionation during land surface evaporation, this always has an enriching effect (Risi et al., 2013). In contrast, boundary-layer mixing is associated with vertical redistribution of moisture, which has a dehydrating and depleting effect on the lower levels.

In LMDZ, the temporal derivatives of q and δD are computed as the sum of different processes. Their contribution is shown in Fig. 11 and in Table 2.

5.1.2 Contribution to humidity variations

At the seasonal scale, the increase of 13 g kg^{-1} in q from spring to summer is associated with a positive and increasing contribution in the "surface evaporation and boundary-layer processes" component, with a maximum of 6 (g kg^{-1}) day^{-1} in July (Fig. 11a). Therefore, surface evaporation drives the moistening in spring. This increased moistening is partly compensated by an increased dehydration caused by summertime deep convection and large-scale advection (about 4 (g kg^{-1}) day^{-1} for both). In autumn, the decrease in q is associated with a negative contribution of the "surface evaporation and boundary-layer processes" component. Therefore, the decrease in surface evaporation likely drives the dehydration in autumn. Advection processes also take part in this decrease with 1 (g kg^{-1}) day^{-1}. Since the boundary layer is expected to be most active in summer, we exclude an increase of boundary-layer mixing as an explanation for the dehydration.

At the daily scale, in summer, q variations correlate the best with the "horizontal advection" component (0.40). In addition, increases in q are associated with spikes in the "surface evaporation and boundary-layer processes" component. Therefore, sur-

ACPD
14, 4457–4503, 2014

face evaporation also drives the daily variability of q in the summer. This is consistent with the important role of continental recycling on q variations diagnosed by Risi et al. (2013).

In winter, variations in q are also mainly associated with variations in the large-scale advection component and "surface evaporation and boundary-layer processes". This is confirmed by the good correlation between q and "advection" and "boundary-layer" tendencies and (r = 0.65 and 0.67 respectively) (Table 2). The importance of advection is consistent with the predominance of synoptic disturbances which modify the direction of the winds. Since evaporation is low during this season, "surface evaporation and boundary-layer processes" are likely associated mostly with boundary-layer processes.

5.1.3 Contribution to δD variations

For δD, the contributions of the different processes to the time derivative mirror those for q (Fig. 11b): most moistening processes act to enrich the water vapor, and vice versa. However, the relative amplitudes of the different processes are different. This supports the idea that δD contributes some independent information compared to q. At the seasonal scale, surface evaporation contributes to the increase in δD in spring and to its decrease in summer, consistent with what we explained for q.

In the winter, boundary-layer processes make the biggest contribution to variations of δD: they are well correlated, with r = 0.59 (Table 2). However, in early spring, large-scale advection also plays a significant role in the enrichment of the water vapor (20–30 ‰ day^{-1}). At the daily level, surface evaporation drives the spikes of δD in summer with maximum in July with 30 ‰ day^{-1}, and large-scale advection is mainly responsible for the δD fluctuations in winter (r = 0.44), consistent with our explanation for q. In summer, the large-scale condensation also plays a slightly enriching role in summer, due to the re-evaporation of rain in the boundary layer. In spring and autumn, large-scale condensation strongly depletes the water vapor on some days. This is consistent with the formation of fog (Noone et al., 2013). These fog events occur on days with strong surface evaporation but relatively stable and shallow boundary layers. On these

ACPD
14, 4457–4503, 2014

days, the depletion by large-scale condensation compensates for the enrichment by surface evaporation.

Thus we can suggest that the boundary-layer dynamics and the large-scale advection control the daily variability of q and isotopic composition especially in winter. In summer, surface evaporation also plays an important role.

5.2 Interpreting model-data differences

The goal of this section is to interpret model-data differences in water isotopic composition, and to investigate what we can learn from water isotopic measurements about the representation of processes in models. We focus here on water vapor δD.

Therefore, we investigate first the model-data differences in q, and then the model-data differences in the relationship of δD vs. ln(q).

5.2.1 Model-data differences in specific humidity

Figure 8a showed that LMDZ tends to estimate q correctly during winter, and underestimate it during summer. The specific humidity (q) can be expressed as a function of temperature (T) and relative humidity (RH): $q = \mathrm{RH} \cdot q_s(T)$, with q_s being the specific humidity at saturation. T reflects mainly dynamical and radiative processes, whereas RH reflects mainly dynamical, surface and cloud processes. Another possible cause of summer underestimation may be fine structure of temperature and humidity vertical profiles at surface which cannot be represented on coarser mesh of LMDZ.

Table 3 shows that on average in winter, LMDZ overestimates q because it overestimates both the temperature (accounting for 72 % of the overestimate of q) and the relative humidity. LMDZ overestimates q the most on days when it overestimates T the most. This occurs mainly during the driest days in the observations. One hypothesis is that LMDZ overestimates the advection of warm and moist air from the south-west during these days.

ACPD
14, 4457–4503, 2014

CC BY

In summer, Table 3 shows that on average, LMDZ underestimates q because it strongly underestimates the relative humidity, although it overestimates the temperature. LMDZ underestimates q the most on days when it is too warm, and this corresponds also to days when LMDZ is too dry. One hypothesis is that LMDZ overestimates the advection of warm and dry air from the south. Another hypothesis is that LMDZ underestimates the surface evapotranspiration. More evapotranspiration would both moisten the atmosphere and cool the surface.

In the next subsection, we will investigate whether water isotopic measurements can help us test these hypotheses.

5.2.2 Model-data differences in the δD – ln(q) relationship

Figure 12a shows daily vapor δD as a function of ln(q). The surface observations cluster along a line, consistent with δD varying along a Rayleigh distillation line (Sect. 2.7). The correlations are high (Table 4). The slopes are twice lower than expected, however, based on the fractionation coefficients and on Eq. (1): 40 to 60 ‰ in the observations depending on the season, compared to 80–120 ‰ expected from fractionation coefficients depending on the condensation temperature. This suggests that δD does not follow a pure distillation line. It might also be affected by mixing processes (Hurley et al., 2012).

If δD is affected by mixing processes, then δD is expected to vary linearly with $1/q$ (Keeling, 1958). To test this hypothesis, we calculate the correlations of δD as a function of $1/q$ (Table 4). Correlations are slightly lower but still very high. Therefore, the influence of mixing processes on δD cannot be completely excluded.

Figure 12 and Table 4 show that LMDZ captures the slopes of the relationship of δD vs. ln(q) reasonably well in summer and in winter. This suggests that the Rayleigh distillation processes, or mixing processes (if they exist), are well represented. However, δD values are systematically offset: LMDZ is systematically more enriched by about 15 ‰ than observations, for a given q. This suggests that the origin of water vapor that undergoes the distillation is not properly represented.

ACPD
14, 4457–4503, 2014

We analyze the relationship between model-data differences in δD and in ln(q) (Fig. 12b). In winter, there is no systematic relationship between model-data differences in δD and those in ln(q). This suggests that the too-large LMDZ enrichment is not related to a Rayleigh distillation that is too weak. Rather, some processes in LMDZ, independent of the Rayleigh distillation, are misrepresented, and they lead to biases in δD that are not directly related to biases in q. We could speculate on different hypotheses, such as moisture origin issues or cloud processes. However, these are difficult to test.

In contrast, in summer, there is a systematic relationship between model-data differences in δD and those in ln(q). When LMDZ has the largest enrichment bias in δD, LMDZ has also the largest moist bias in q. When LMDZ has a depleted bias in δD, LMDZ has the largest dry bias in q. Furthermore, the slope of the relationship between $\Delta\delta$D and Δln(q) is similar to that between δD and q (Table 4). Therefore, the model-data differences in δD are probably due to the same processes as those controlling the daily variability of δD in nature. More specifically, the biases in q could be due to the Rayleigh distillation, to a contribution of strongly dehydrated and distilled air from the south or to a contribution from surface evapotranspiration being too strong or too weak depending on the day.

To summarize, analyzing observations and model-data differences in δD vs. ln(q) plots reveals some information about the sources of model biases, though it does not allow us to pinpoint them with certainty. The model is systematically too enriched all year long probably due to a moisture origin issue. In winter, the δD bias is modulated on a daily basis by processes that are independent from the Rayleigh distillation. In summer, the δD bias is modulated by the same processes as those explaining the daily variability in surface observations.

ACPD
14, 4457–4503, 2014

6 Conclusions

In this paper, we evaluate the isotopic composition of water vapor and precipitation simulated by the LMDZ GCM over Siberia using several datasets: TES and GOSAT satellite observations of tropospheric water vapor, GNIP and SNIP networks of precipitation, and daily, in-situ measurements of water vapor and precipitation at the Kourovka site in Western Siberia.

LMDZ captures the spatial, seasonal and daily variations reasonably well, except for a few features. LMDZ overestimates the δD in precipitation compared to the precipitation networks, by about 20 ‰. Consistently with this result, LMDZ overestimates the δD observed in both the vapor and precipitation at Kourovka. Based on the analysis of δD vs. humidity diagrams, this bias is most likely associated with a problem with the vapor origin. LMDZ slightly underestimates the latitudinal gradient in δD compared to satellite datasets. LMDZ also underestimates the seasonality in the lower and middle troposphere at Kourovka compared to satellite datasets, but not at the surface compared to the in-situ data. Finally, LMDZ captures some aspects of the spatial and daily variations in d-excess.

The performance of LMDZ in capturing the spatial and seasonal variations in δD is consistent with other state-of-the-art models participating in the SWING2 intercomparison project. There is a large spread in the simulation of the latitudinal and seasonal variations in δD, which is not explained by the spread in the simulation of q. This confirms the added value of deuterium measurements compared to q measurements only, though we still need to make progress to better understand why there are systematic biases in δD in models and why different models simulate different δD variations.

Using LMDZ to investigate the processes controlling the daily variability, we find that two processes dominate. First, the large-scale advection determines origin of the moisture, enriched in the south and west and depleted in the north and east. Second, surface evaporation and boundary layer processes determine the proportion of the vapor coming from enriched surface evaporation or from the more depleted free troposphere.

ACPD
14, 4457–4503, 2014

CC BY

Most GCMs suffer from a warm and dry bias over mid-latitude continents in summer. LMDZ shares this same bias. In addition to a systematic bias towards too enriched δD values, LMDZ exhibits the strongest dry bias on days when it simulates the strongest enriched bias in δD. Moreover, the slope of δD biases vs. q biases is consistent with the slope of δD vs. q in observations. This suggests that the same processes that explain the joint δD and q variability explain the biases in q. Therefore, the cause of the dry bias could be either a problem in the large-scale advection bringing too much dry and warm air from the south, or insufficient surface evaporation.

This paper shows the potential of combining δD and humidity measurements in δD vs. q or logarithm-of-humidity diagrams, to interpret model-data and model-model differences in terms of the representation of physical processes. However, even using such diagrams, it is difficult to discriminate for sure between Rayleigh lines and mixing lines between different kinds of end members. More work is needed to better constrain such theoretical lines in particular the composition of their end members. A better spatial coverage of water vapor isotopic measurements would be useful for documenting the composition of end members that are water vapors coming from different origins. Measuring vertical gradient in isotopic composition would be useful for documenting the composition of the evapotranspiration member. Finally, more precise measurement and a better understanding of d-excess could add an additional constraint to the system of isotopic equations that has so far suffered from too many unknowns compared to the number of equations.

Acknowledgements. This research was supported by the grants of Russian government under the contract 11.G34.31.0064 and the project #2189 within the State tasks (base part) of the High Education Ministry of Russian Federation. The authors would like to thank Francesca Guglielmo and Laura Kerber for their helpful comments and discussions. Part of this research was carried out at the Jet Propulsion Laboratory, California Institute of Technology, under a contract with the National Aeronautics and Space Administration.

References

Bastrikov, V., Steen-Larsen, H. C., Masson-Delmotte, V., Gribanov, K., Cattani, O., Jouzel, J., and Zakharov, V.: Continuous measurements of atmospheric water vapour isotopes in Western Siberia (Kourovka), Atmos. Meas. Tech. Discuss., 7, 475–507, doi:10.5194/amtd-7-475-2014, 2014.

Bellprat, O., Kotlarski, S., Lüthi, D., and Schär, C.: Physical constraints for temperature biases in climate models, Geophys. Res. Lett., 40, 4042–4047, 2013.

Boberg, F. and Christensen, J. H.: Overestimation of Mediterranean summer temperature projections due to model deficiencies, Nat. Clim. Chang., 2, 433–436, 2012.

Boé, J.: Modulation of soil moisture-precipitation interactions over France by large scale circulation, Clim. Dynam., 40, 875–892, 2013.

Boé, J. and Terray, L.: Uncertainties in summer evapotranspiration changes over Europe and implications for regional climate change, Geophys. Res. Lett., 35, L05702, doi:10.1029/2007GL032417, 2008.

Bony, S., Risi, C., and Vimeux, F.: Influence of convective processes on the isotopic composition (δ^{18}O and δD) of precipitation and water vapor in the tropics: 1. Radiative-convective equilibrium and Tropical Ocean-Global Atmosphere-Coupled Ocean-Atmosphere Response Experiment (TOGA-COARE) simulations, J. Geophys. Res., 113, D19305, doi:10.1029/2008JD009942, 2008.

Butzin, M., Werner, M., Masson-Delmotte, V., Risi, C., Frankenberg, C., Gribanov, K., Jouzel, J., and Zakharov, V. I.: Variations of oxygen-18 in West Siberian precipitation during the last 50 yr, Atmos. Chem. Phys. Discuss., 13, 29263–29301, doi:10.5194/acpd-13-29263-2013, 2013.

Cattiaux, J., Douville, H., and Peings, Y.: European temperatures in CMIP5: origins of present-day biases and future uncertainties, Clim. Dyn., 41, 2889–2907, doi:10.1007/s00382-013-1731-y, 2013.

Cheruy, F., Campoy, A., Dupont, J. C., Ducharne, A., Hourdin, F., Haeffelin, M., Chiriaco, M., and Idelkadi, A.: Combined influence of atmospheric physics and soil hydrology on the simulated meteorology at the SIRTA atmospheric observatory, Clim. Dynam., 40, 2251–2269, 2013.

Christensen, J. H. and Boberg, F.: Temperature dependent climate projection deficiencies in CMIP5 models, Geophys. Res. Lett., 39, L24705, doi:10.1029/2012GL053650, 2012.

Craig, H.: Isotopic variations in meteoric waters, Science, 133, 1702–1703, 1961.

ACPD
14, 4457–4503, 2014

Dansgaard, W.: Stable isotopes in precipitation, Tellus, 16, 436–468, 1964.
Folkins, I. and Martin, R. V.: The vertical structure of tropical convection and its impact on the budgets of water vapor and ozone, J. Atmos. Sci., 62, 1560–1573, 2005.
Frankenberg, C., Yoshimura, K., Warneke, T., Aben, I., Butz, A., Deutscher, N., Griffith, D., Hase, F., Notholt, J., Schneider, M., Schrijver, H., and Röckmann, T.: Dynamic processes governing lower-tropospheric HDO/H_2O ratios as observed from space and ground, Science, 325, 1374–1377, 2009.
Frankenberg, C., Wunch, D., Toon, G., Risi, C., Scheepmaker, R., Lee, J.-E., Wennberg, P., and Worden, J.: Water vapor isotopologue retrievals from high-resolution GOSAT shortwave infrared spectra, Atmos. Meas. Tech., 6, 263–274, doi:10.5194/amt-6-263-2013, 2013.
Galewsky, J. and Hurley, J. V.: An advection-condensation model for subtropical water vapor isotopic ratios, J. Geophys. Res., 115, D16116, doi:10.1029/2009JD013651, 2010.
Gat, J. R. and Matsui, E.: Atmospheric water balance in the Amazon basin: an isotopic evapotranspiration model, J. Geophys. Res., 96, 13179–13188, 1991.
Hourdin, F., Musat, I., Bony, S., Braconnot, P., Codron, F., Dufresne, J.-L., Fairhead, L., Filiberti, M.-A., Friedlingstein, P., Grandpeix, J.-Y., Krinner, G., LeVan, P., Li, Z.-X., and Lott, F.: The LMDZ4 general circulation model: climate performance and sensitivity to parametrized physics with emphasis on tropical convection, Clim. Dynam., 27, 787–813, 2006.
Hurley, J. V., Galewsky, J., Worden, J., and Noone, D.: A test of the advection-condensation model for subtropical water vapor using stable isotopologue observations from Mauna Loa Observatory, Hawaii, J. Geophys. Res.-Atmos., 117, D19118, doi:10.1029/2012JD018029, 2012.
Jouzel, J. and Koster, R. D.: A reconsideration of the initial conditions used for stable water isotope models, J. Geophys. Res.-Atmos., 101, 22933–22938, 1996.
Jouzel, J. and Merlivat, L.: Deuterium and oxygen 18 in precipitation: modeling of the isotopic effects during snow formation, J. Geophys. Res., 89, 11749–11757, 1984.
Keeling, C. D.: The concentration and isotopic abundances of atmospheric carbon dioxide in rural areas, Geochim. Cosmochim. Ac., 13, 322–334, 1958.
Kittel, T. G. F., Giorgi, F., and Meehl, G. A.: Intercomparsion of regional biases and doubled CO_2-sensitivity of coupled atmosphere-ocean general circulation model experiments, Clim. Dynam., 14, 1–15, 1997.

ACPD
14, 4457–4503, 2014

Klein, S. A., Jiang, X., Boyle, J., Malyshev, S., and Xie, S.: Diagnosis of the summertime warm and dry bias over the US southern Great Plains in the GFDL climate model using a weather forecasting approach, Geophys. Res. Lett., 33, L18805, doi:10.1029/2006GL027567, 2006.

Kurita, N., Yoshida, N., Inoue, G., and Chayanova, E. A.: Modern isotope climatology of Russia: a first assessment, J. Geophys. Res., 109, D03102, doi:10.1029/2003JD003404, 2004.

Lawrence, J. R., Gedzelman, S. D., Dexheimer, D., Cho, H.-K., Carrie, G. D., Gasparini, R., Anderson, C. R., Bowman, K. P., and Biggerstaff, M. I.: Stable isotopic composition of water vapor in the tropics, J. Geophys. Res.-Atmos., 109, D06115, doi:10.1029/2003JD004046, 2004.

Lee, J.-E., Pierrehumbert, R., Swann, A., and Lintner, B. R.: Sensitivity of stable water isotopic values to convective parameterization schemes, Geophys. Res. Lett., 36, L23801, doi:10.1029/2009GL040880, 2009.

Majoube, M.: Fractionnement en oxygene-18 et en deuterium entre l'eau et sa vapeur, J. Chim. Phys., 68, 1423–1436, 1971a.

Majoube, M.: Fractionnement en oxygene 18 entre la glace et la vapeur d'eau, J. Chem. Phys., 68, 625–636, 1971b.

Masson-Delmotte, V., Hou, S., Ekaykin, A., Jouzel, J., Aristarain, A., Bernardo, R. T., Bromwich, D., Cattani, O., Delmotte, M., Falourd, S., Frezzotti, M., Gallée, H., Genoni, L., Isaksson, E., Landais, A., Helsen, M. M., Hoffmann, G., Lopez, J., Morgan, V., Motoyama, H., Noone, D., Oerter, H., Petit, J. R., Royer, A., Uemura, R., Schmidt, G. A., Schlosser, E., Simões, J. C., Steig, E. J., Stenni, B., Stievenard, M., van den Broeke, M. R., van de Wal, R. S. W., van de Berg, W. J., Vimeux, F., and White, J. W. C.: A review of Antarctic surface snow isotopic composition: observations, atmospheric circulation and isotopic modelling, J. Climate, 21, 3359–3387, 2008.

Meehl, G. A., Covey, C., Taylor, K. E., Delworth, T., Stouffer, R. J., Latif, M., McAvaney, B., and Mitchell, J. F. B.: The WCRP CMIP3 multi-model dataset: a new era in climate change research, B. Am. Meteorol. Soc., 88, 1383–1394, 2007.

Merlivat, L. and Jouzel, J.: Global climatic interpretation of the deuterium-oxygen 18 relationship for precipitation, J. Geophys. Res., 84, 5029–5033, 1979.

Merlivat, L. and Nief, G.: Fractionnement isotopique lors des changements d'état solide-vapeur et liquide-vapeur de l'eau à des températures inférieures à 0 °C, Tellus, 19, 122–127, 1967.

ACPD
14, 4457–4503, 2014

Moberg, A. and Jones, P.: Regional climate model simulations of daily maximum and minimum near-surface temperatures across Europe compared with observed station data 1961–1990, Clim. Dynam., 23, 695–715, 2004.

Noone, D., Risi, C., Bailey, A., Berkelhammer, M., Brown, D. P., Buenning, N., Gregory, S., Nusbaumer, J., Schneider, D., Sykes, J., Vanderwende, B., Wong, J., Meillier, Y., and Wolfe, D.: Determining water sources in the boundary layer from tall tower profiles of water vapor and surface water isotope ratios after a snowstorm in Colorado, Atmos. Chem. Phys., 13, 1607–1623, doi:10.5194/acp-13-1607-2013, 2013.

Polcher, J., Laval, K., Dümenil, L., Lean, J., and Rowntree, P. R.: Comparing three land surface schemes used in general circulation models, J. Hydrol., 180, 373–394, 1996.

Pommier, M., Lacour, J.-L., Risi, C., Bréon, F.-M., Clerbaux, C., Coheur, P.-F., Gribanov, K., Hurtmans, D., Jouzel, J., and Zakharov, V.: Observation of tropospheric δ D by IASI over the Western Siberia: comparison with a GCM, Atmos. Meas. Tech. Discuss., 6, 11055–11092, doi:10.5194/amtd-6-11055-2013, 2013.

Risi, C., Bony, S., and Vimeux, F.: Influence of convective processes on the isotopic composition (δ^{18}O and δD) of precipitation and water vapor in the tropics: 2. Physical interpretation of the amount effect, J. Geophys. Res., 113, D19306, doi:10.1029/2008JD009943, 2008.

Risi, C., Bony, S., Vimeux, F., Chong, M., and Descroix, L.: Evolution of the stable water isotopic composition of the rain sampled along Sahelian squall lines, Q. J. Roy. Meteor. Soc., 136, 227–242, 2010a.

Risi, C., Bony, S., Vimeux, F., and Jouzel, J.: Water-stable isotopes in the LMDZ4 general circulation model: model evaluation for present-day and past climates and applications to climatic interpretations of tropical isotopic records, J. Geophys. Res., 115, D12118, doi:10.1029/2009JD013255, 2010b.

Risi, C., Noone, D., Worden, J., Frankenberg, C., Stiller, G., Kiefer, M., Funke, B., Walker, K., Bernath, P., Schneider, M., Bony, S., Lee, J., Brown, D., and Sturm, C.: Process-evaluation of tropospheric humidity simulated by general circulation models using water vapor isotopic observations: 2. Using isotopic diagnostics to understand the mid and upper tropospheric moist bias in the tropics and subtropics, J. Geophys. Res., 117, D05304, doi:10.1029/2011JD016623, 2012a.

Risi, C., Noone, D., Worden, J., Frankenberg, C., Stiller, G., Kiefer, M., Funke, B., Walker, K., Bernath, P., Schneider, M., Wunch, D., Sherlock, V., Deutscher, N., Griffith, D., Wennberg, P. O., Strong, K., Smale, D., Mahieu, E., Barthlott, S., Hase, F., García, O.,

Notholt, J., Warneke, T., Toon, G., Sayres, D., Bony, S., Lee, J., Brown, D., Uemura, R., and Sturm, C.: Process-evaluation of tropospheric humidity simulated by general circulation models using water vapor isotopologues: 1. Comparison between models and observations, J. Geophys. Res., 117, D05303, doi:10.1029/2011JD016621, 2012b.

Risi, C., Noone, D., Frankenberg, C., and Worden, J.: Role of continental recycling in intraseasonal variations of continental moisture as deduced from model simulations and water vapor isotopic measurements, Water Resour. Res., 49, 4136–4156, 2013.

Rozanski, K., Araguás-Araguás, L., and Gonfiantini, R.: Isotopic patterns in modern global precipitation, in: Climate change in continental isotopic records, Geophys. Monogr. Ser., 78, AGU, Washington, DC, 1–36, 1993.

Salati, E., Dall'Olio, A., Matsui, E., and Gat, J. R.: Recycling of water in the Amazon Basin: an isotopic study, Water Resour. Res., 15, 1250–1258, 1979.

Schneider, M., Yoshimura, K., Hase, F., and Blumenstock, T.: The ground-based FTIR network's potential for investigating the atmospheric water cycle, Atmos. Chem. Phys., 10, 3427–3442, doi:10.5194/acp-10-3427-2010, 2010.

Simonin, K. A., Link, P., Rempe, D., Miller, S., Oshun, J., Bode, C., Dietrich, W. E., Fung, I., and Dawson, T. E.: Vegetation induced changes in the stable isotope composition of near surface humidity, Ecohydrol., doi:10.1002/eco.1420, 2013.

Steen-Larsen, H. C., Johnsen, S. J., Masson-Delmotte, V., Stenni, B., Risi, C., Sodemann, H., Balslev-Clausen, D., Blunier, T., Dahl-Jensen, D., Ellehøj, M. D., Falourd, S., Grindsted, A., Gkinis, V., Jouzel, J., Popp, T., Sheldon, S., Simonsen, S. B., Sjolte, J., Steffensen, J. P., Sperlich, P., Sveinbjörnsdóttir, A. E., Vinther, B. M., and White, J. W. C.: Continuous monitoring of summer surface water vapor isotopic composition above the Greenland Ice Sheet, Atmos. Chem. Phys., 13, 4815–4828, doi:10.5194/acp-13-4815-2013, 2013.

Stewart, M. K.: Stable isotope fractionation due to evaporation and isotopic exchange of falling waterdrops: applications to atmospheric processes and evaporation of lakes, J. Geophys. Res., 80, 1133–1146, 1975.

Uppala, S. M., KÅllberg, P. W., Simmons, A. J., Andrae, U., Bechtold, V. D. C., Fiorino, M., Gibson, J. K., Haseler, J., Hernandez, A., Kelly, G. A., Li, X., Onogi, K., Saarinen, S., Sokka, N., Allan, R. P., Andersson, E., Arpe, K., Balmaseda, M. A., Beljaars, A. C. M., Berg, L. V. D., Bidlot, J., Bormann, N., Caires, S., Chevallier, F., Dethof, A., Dragosavac, M., Fisher, M., Fuentes, M., Hagemann, S., Hólm, E., Hoskins, B. J., Isaksen, L., Janssen, P. A. E. M., Jenne, R., McNally, A. P., Mahfouf, J. F., Morcrette, J. J., Rayner, N. A., Saunders, R. W.,

Simon, P., Sterl, A., Trenberth, K. E., Untch, A., Vasiljevic, D., Viterbo, P., and Woollen, J.: The ERA-40 re-analysis, Q. J. Roy. Meteor. Soc., 131, 2961–3012, 2005.

Worden, J., Kulawik, S., Frankenberg, C., Payne, V., Bowman, K., Cady-Peirara, K., Wecht, K., Lee, J.-E., and Noone, D.: Profiles of CH_4, HDO, H_2O, and N_2O with improved lower tropospheric vertical resolution from Aura TES radiances, Atmos. Meas. Tech., 5, 397–411, doi:10.5194/amt-5-397-2012, 2012.

Worden, J., Noone, D., and Bowman, K.: Importance of rain evaporation and continental convection in the tropical water cycle, Nature, 445, 528–532, 2007.

Worden, J., Noone, D., Galewsky, J., Bailey, A., Bowman, K., Brown, D., Hurley, J., Kulawik, S., Lee, J., and Strong, M.: Estimate of bias in Aura TES HDO/H_2O profiles from comparison of TES and in situ HDO/H_2O measurements at the Mauna Loa observatory, Atmos. Chem. Phys., 11, 4491–4503, doi:10.5194/acp-11-4491-2011, 2011.

Worden, J., Bowman, K., Noone, D., Beer, R., Clough, S., Eldering, A., Fisher, B., Goldman, A., Gunson, M., Herman, R., Kulawik, S. S., Lampel, M., Luo, M., Osterman, G., Rinsland, C., Rodgers, C., Sander, S., Shephard, M., and Worden, H.: Tropospheric Emission Spectrometer observations of the tropospheric HDO/H_2O ratio: estimation approach and characterization, J. Geophys. Res., 111, D16309, doi:16310.11029/12005JD006606, 2006.

Yoshimura, K., Kanamitsu, M., Noone, D., and Oki, T.: Historical isotope simulation using Reanalysis atmospheric data, J. Geophys. Res.-Atmos., 113, D19108, doi:10.1029/2008JD010074, 2008.

Yoshimura, K., Kanamitsu, M., and Dettinger, M.: Regional downscaling for stable water isotopes: a case study of an atmospheric river event, J. Geophys. Res., 115, D18114, doi:10.1029/2010JD014032, 2010.

Zipser, E. J.: Mesoscale and convective scale downdrafts as distinct components of squall-line structure, Mon. Weather Rev., 105, 1568–1589, 1977.

ACPD
14, 4457–4503, 2014

Table 1. Daily Pearson correlation coefficient (r) and its significance (p value) for observations in Kourovka and results of simulation by LMDZ-iso calculated to humidity (q), water vapor δD, δ^{18}O, d-excess and difference between precipitation and water vapor. At DJF season data available only for December. If p value is lower than the conventional 5 % then we assume that the correlation coefficient is statistically significant. N/S means "not significant".

	Vapor						Precip-Vapor	
	JJA		DJF		Entire period		Entire period	
	r	p value	r	p value	r	p value	r	p value
q	0.63	< 1 %	0.94	< 1 %	0.90	< 1 %	N/A	N/A
δD	0.54	< 1 %	0.89	< 1 %	0.95	< 1 %	0.47	< 5 %
δ^{18}O	0.55	< 1 %	0.89	< 1 %	0.94	< 1 %	0.32	N/S
d-excess	N/A	N/A	0.27	N/S	0.27	< 1 %	0.26	N/S

ACPD
14, 4457–4503, 2014

Table 2. Daily Pearson correlation coefficient (r), its significance (p value) and the ratio of standard deviations for temporal derivatives and tendencies from different processes simulated by LMDZ-iso ($\sigma_{tend}/\sigma_{td}$): horizontal advection (adv), deep convection (conv), large-scale condensation and re-evaporation (cond), surface evaporation and boundary-layer dynamics (evap). N/S means "not significant".

Temporal derivatives	Tendencies	Annual			DJF			JJA		
		r	p value	$\frac{\sigma_{tend}}{\sigma_{td}}$	r	p value	$\frac{\sigma_{tend}}{\sigma_{td}}$	r	p value	$\frac{\sigma_{tend}}{\sigma_{td}}$
q	adv	0.47	< 1 %	1.36	0.65	< 1 %	0.79	0.40	< 1 %	1.68
	conv	0.06	N/S	1.09	N/A	N/A	N/A	0.03	N/S	1.42
	cond	0.07	N/S	0.19	0.16	N/S	0.24	0.15	N/S	0.22
	evap	0.26	< 1 %	1.76	0.67	< 1 %	0.97	0.16	N/S	2.18
δD	adv	0.40	< 1 %	1.05	0.44	< 1 %	0.87	0.30	< 1 %	1.31
	conv	0.06	N/S	0.56	N/A	N/A	N/A	0.20	< 5 %	1.52
	cond	0.11	< 5 %	1.77	0.08	N/S	0.31	0.31	< 1 %	0.52
	evap	0.31	< 1 %	2.01	0.59	< 1 %	1.28	0.17	N/S	2.03

ACPD
14, 4457–4503, 2014

Table 3. Understanding the model-data differences in specific humidity. The Δ sign refers to the model-data difference.

Season	DJF	JJA
Mean Δq	0.52	−2.0
Mean Δq attributed to ΔT	0.33	2.3
Mean Δq attributed to ΔRH	0.13	−3.3
Correlation between Δq and ΔT	0.91	−0.52
Correlation between Δq and ΔRH	0.68	0.80
Correlation between Δq and q	−0.71	−0.77

ACPD
14, 4457–4503, 2014

Table 4. Relationships between δD and q and between $\Delta\delta$D and $\Delta\ln(q)$. The Δ sign refers to the model-data difference. N/S means "not significant".

Season	Annual	DJF	JJA
Correlation δD vs. $\ln(q)$ observations	0.95	0.93	0.87
Correlation δD vs. $1/q$ observations	−0.84	−0.90	−0.85
Correlation δD vs. $\ln(q)$ LMDZ	0.96	0.97	0.88
Correlation δD vs. $1/q$ LMDZ	−0.90	−0.95	−0.87
Correlation $\Delta\delta$D vs. $\Delta\ln(q)$	0.39	0.11	0.87
Slope δD vs. $\ln(q)$ observations	49.9	37.3	47.5
Slope δD vs. $\ln(q)$ LMDZ	64.4	61.2	49.3
Slope $\Delta\delta$D vs. $\Delta\ln(q)$	21.4	N/S	50.7
Intercept δD vs. $\ln(q)$ observations	−260	−259	−248
Intercept δD vs. $\ln(q)$ LMDZ	−244	−245	−211
Intercept $\Delta\delta$D vs. $\Delta\ln(q)$	26	N/S	41

ACPD
14, 4457–4503, 2014

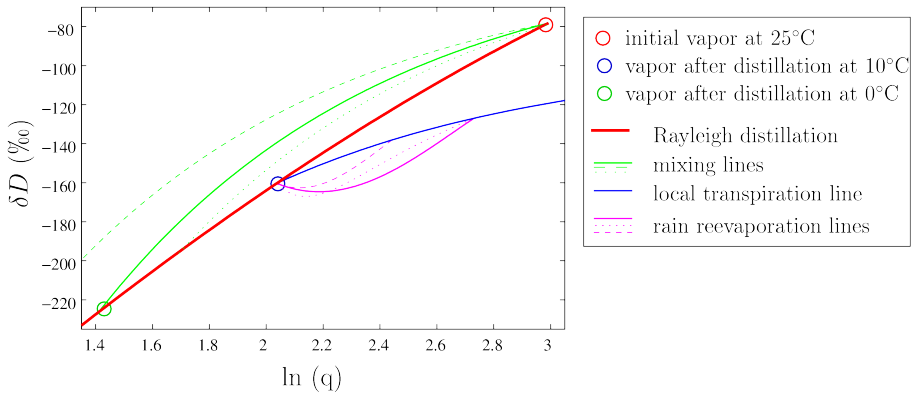

ACPD
14, 4457–4503, 2014

Fig. 1. Theoretical lines in the δD vs. ln(q) plot. The initial vapor (red circle) is assumed to be formed over ocean, with a surface temperature of 25 °C and surface relative humidity of 70 % according to the Merlivat and Jouzel (1979) closure assumption. This vapor follows a Rayleigh distillation following Eq. (1) (red line). The green lines show mixing lines between the initial vapor and a vapors distilled down to different temperatures: 0 °C (thick line), −5 °C (dashed line) and 5 °C (dotted line). These lines are similar to those in Worden et al. (2007). The blue and pink lines show mixing lines between vapor distilled down to 10 °C and the re-evaporation of rain. We assume that the rain is in equilibrium with the overlying vapor. The blue line represents the evaporation of rain without any fractionation, as is the case for transpiration of soil water. The pink lines represents the evaporation of rain with fractionation, following Stewart (1975) and Bony et al. (2008): re-evaporation of rain in an equal amount of water vapor with air humidity of 70 % (solid), in an equal amount of water vapor with 90 % humidity (dotted) or in a twice larger amount of water vapor with 70 % humidity (dashed). Note that these re-evaporation lines are different from those in Worden et al. (2007), because they neglected the evolution of the raindrop composition during re-evaporation, whereas we do a more precise calculation, and because they plotted a combination of distillation and re-evaporation, whereas we plotted the effect of re-evaporation only.

ACPD
14, 4457–4503, 2014

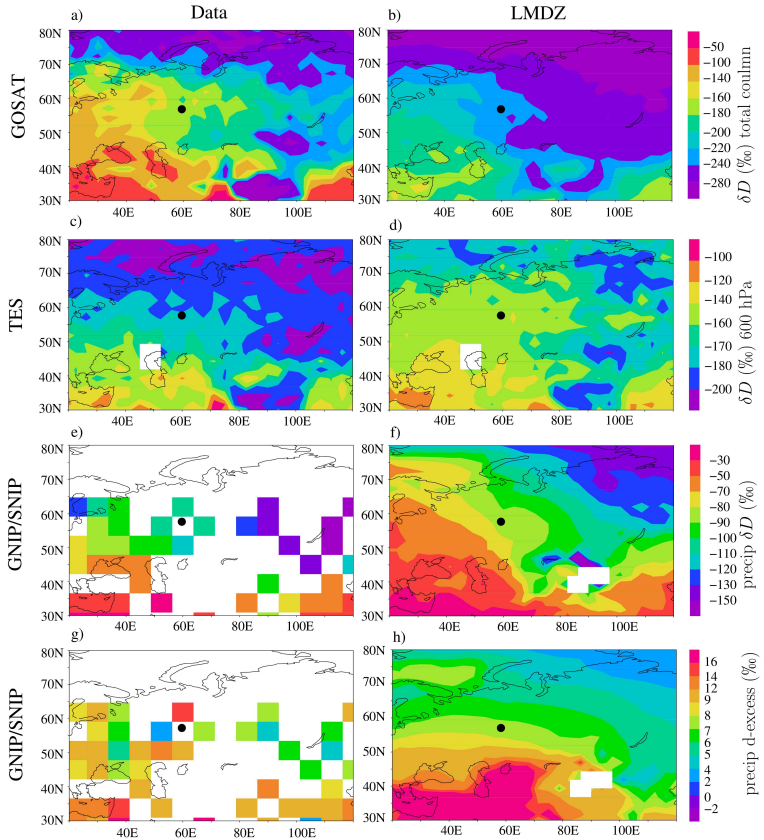

Fig. 2. Annual mean maps of observed (left) and simulated (right) δD in the total column water vapor as observed by GOSAT **(a–b)**, and by TES **(c–d)**, δD in the surface precipitation **(e–f)** and d-excess in the surface precipitation **(g–h)**. The black dot indicates the location of Kourovka.

ACPD
14, 4457–4503, 2014

CC BY

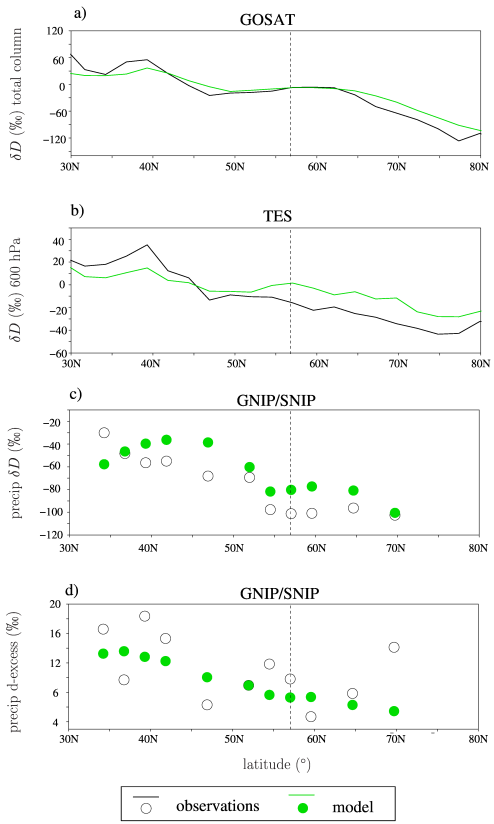

Fig. 3. Annual mean north-south transects of observed (black) and simulated (green) δD in the total column water vapor as observed by GOSAT **(a)** and by TES **(b)**, δD in the surface precipitation **(c)** and d-excess in the surface precipitation **(d)**. Transects are taken around the longitude of Kourovka: 50° E–70° E. For satellite datasets, the annual-mean δD averaged over 50° E–70° E – 30° N–80° N is subtracted to focus on the latitudinal variations. LMDZ simulated outputs were collocated with each dataset. The dashed line indicates the latitude of Kourovka.

ACPD
14, 4457–4503, 2014

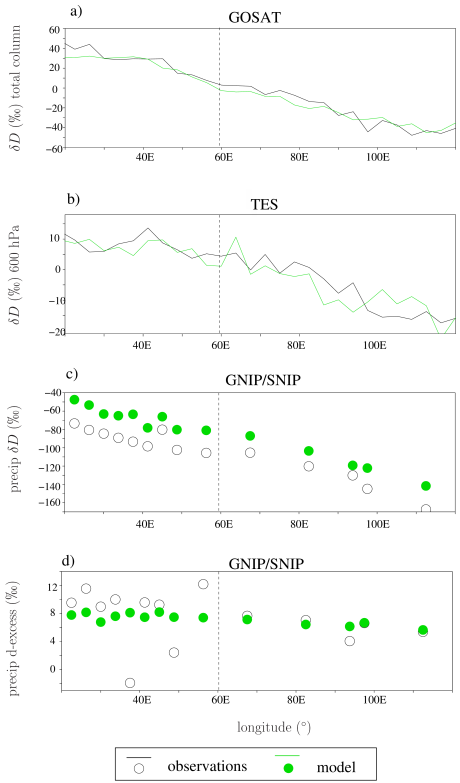

Fig. 4. Annual mean east-west transects of observed (black) and simulated (green) δD in the total column water vapor as observed by GOSAT **(a)** and by TES **(b)**, δD in the surface precipitation **(c)** and d-excess in the surface precipitation **(d)**. Transects are taken around the latitude of Kourovka: 50° N–64° N. For satellite datasets, the annual-mean δD averaged over 20° E–120° E – 50° N–64° N is subtracted to focus on the longitudinal variations. LMDZ simulated outputs were collocated with each dataset. The dashed line indicates the longitude of Kourovka.

ACPD
14, 4457–4503, 2014

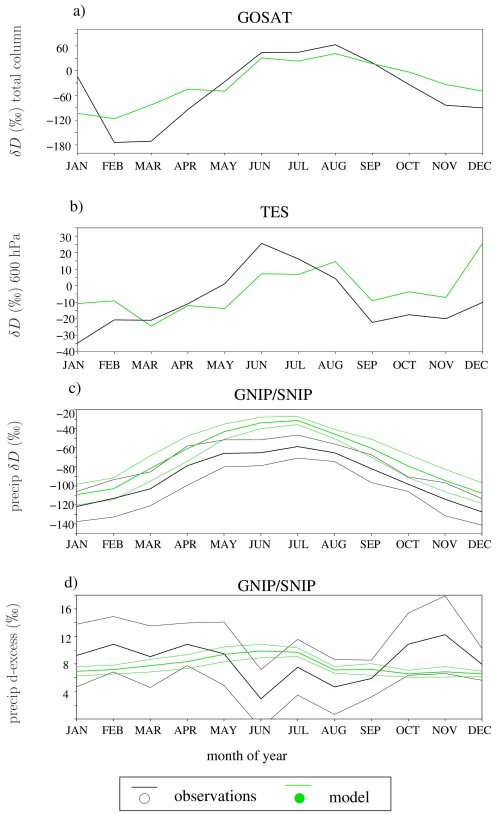

Fig. 5. Seasonal cycles of observed (black) and simulated (green) δD in the total column water vapor **(a)**, δD in the vapor at 600 hPa **(b)**, δD in the surface precipitation **(c)** and d-excess in the surface precipitation **(d)**. We average over the region of Kourovka (50° N–64° N – 50° E–70° E). For satellite datasets, the annual-mean δD is subtracted to focus on the seasonal variations. For GNIP/SNIP datasets, the spatial standard deviation is also plotted as an envelope. LMDZ simulated outputs were collocated with each dataset.

ACPD
14, 4457–4503, 2014

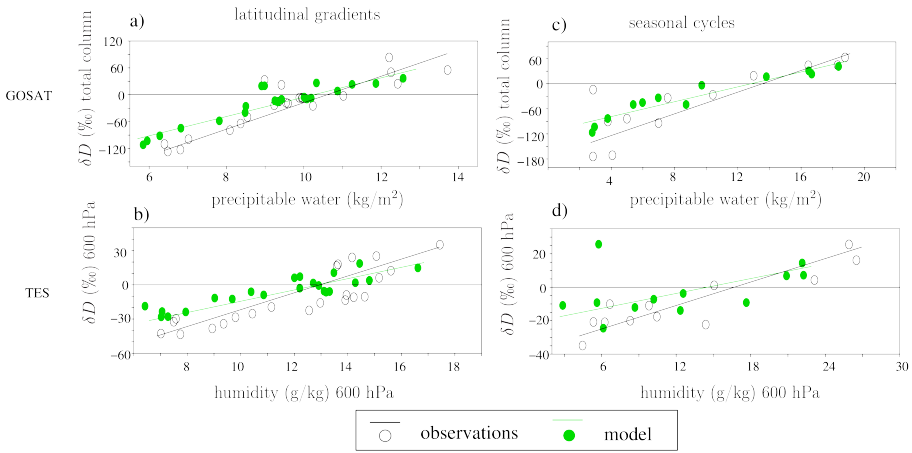

Fig. 6. (a) Total column water vapor δD as a function of precipitable water as observed by GOSAT (black) and as simulated by LMDZ (green) along the latitudinal transects plotted on Fig. 3; **(b)** same as **(a)** but for seasonal cycles as plotted on Fig. 5; **(c–d)** same as **(a–b)** but as observed by TES. Temporal and spatial averages are all the same as in Figs. 3 and 5.

ACPD
14, 4457–4503, 2014

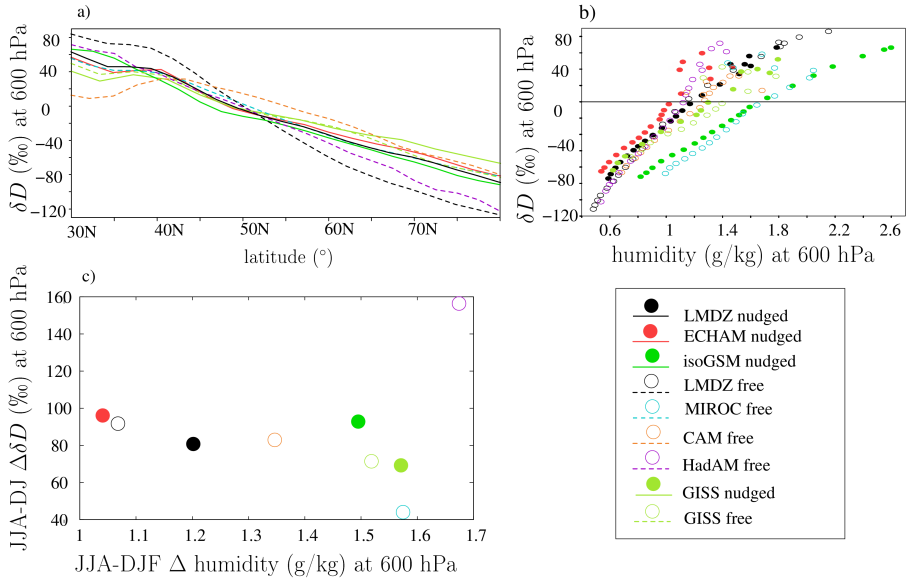

Fig. 7. (a) Annual mean north-south transects of water vapor δD at 600 hPa simulated by different SWING2 models. Transects are taken around the longitude of Kourovka: 50° E–70° E. The annual-mean δD averaged over 50° E–70° E – 30° N–80° N is subtracted to focus on the latitudinal variations. The spatial averaging are the same as in Fig. 3. **(b)** Water vapor δD at 600 hPa as a function of humidity at 600 hPa. **(c)** Seasonal amplitudes (June-July-August minus December-January-February) of δD at 600 hPa in the region of Kourovka (50° N–64° N – 50° E–70° E), as a function of the seasonal amplitude in humidity at 600 hPa.

ACPD
14, 4457–4503, 2014

CC BY

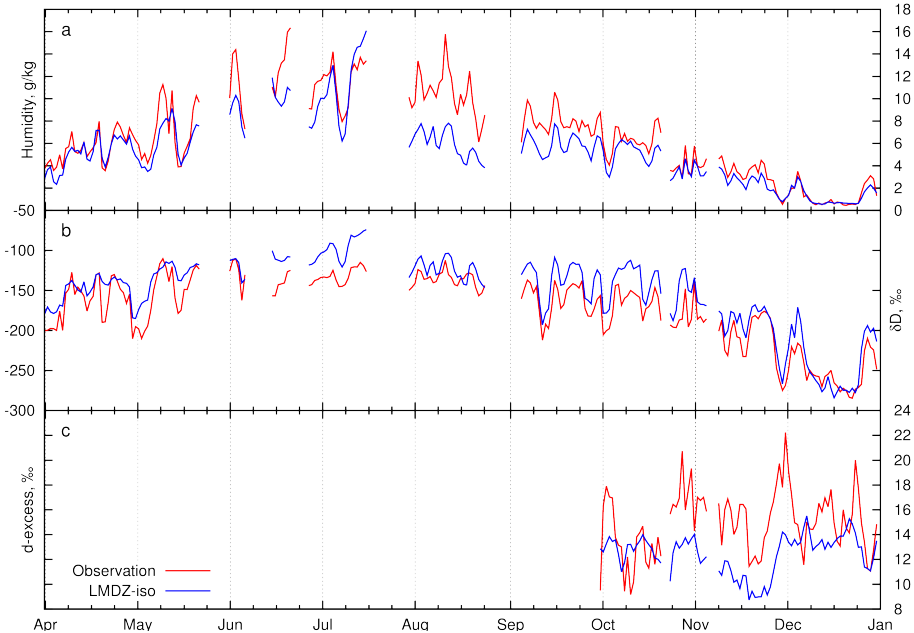

Fig. 8. Daily mean timeseries of humidity **(a)**, water vapor δD **(b)** and d-excess **(c)** for observations in Kourovka (red) and simulated by LMDZ-iso (blue).

ACPD
14, 4457–4503, 2014

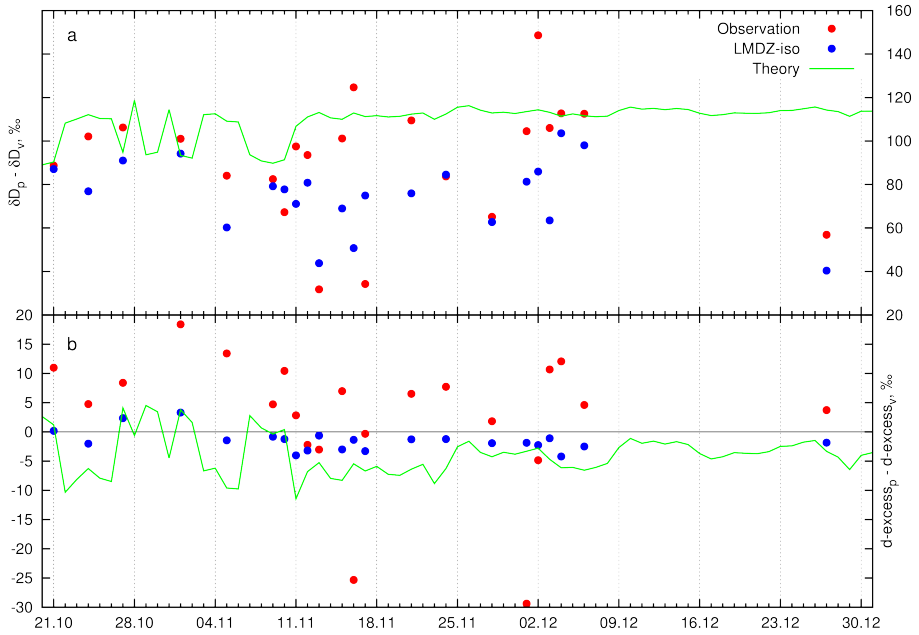

Fig. 9. Daily mean difference between precipitation and water vapor δD **(a)** and d-excess **(b)** for observations in Kourovka (red) and LMDZ-iso (blue). The green line represents a theoretical estimation of this difference.

ACPD
14, 4457–4503, 2014

CC BY

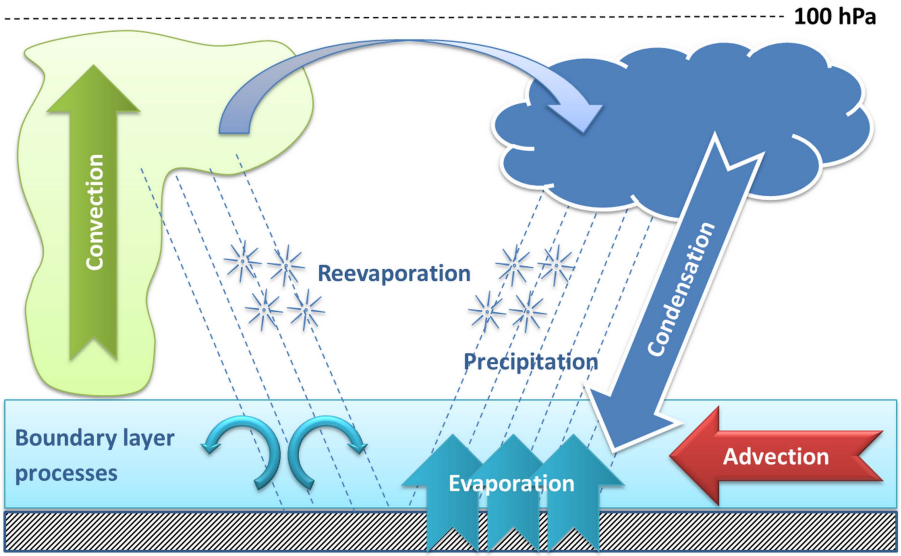

Fig. 10. Schematic representation of the hydrological cycle which includes physical process: advection, deep convection, large-scale condensation, re-evaporation, surface evaporation and boundary-layer processes.

ACPD
14, 4457–4503, 2014

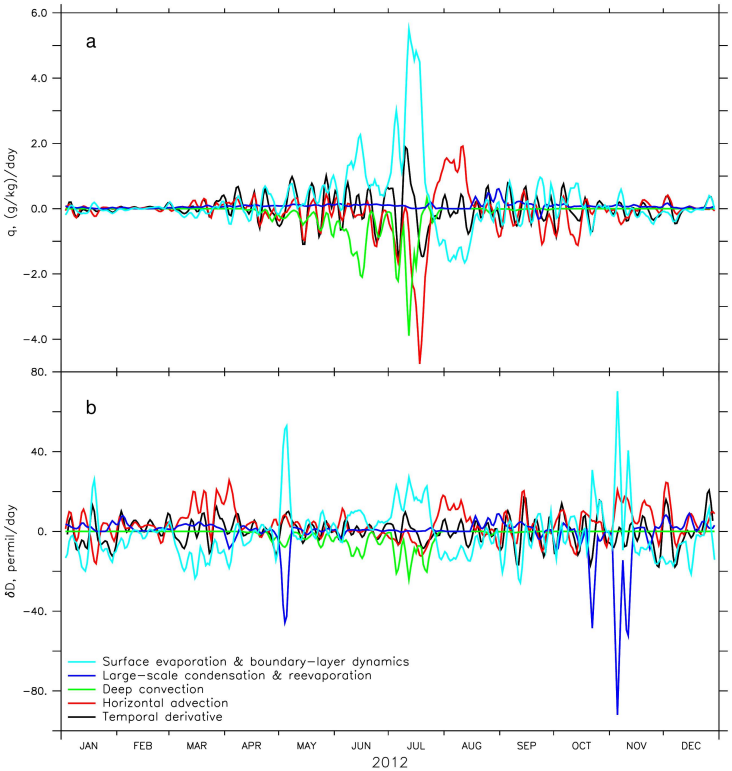

Fig. 11. Temporal derivative (black line) of **(a)** humidity and **(b)** δD at the surface simulated by LMDZ-iso. This temporal derivative can be decomposed into the tendencies from different processes (illustrated on Fig. 10): horizontal advection (red); deep convection (green); large-scale condensation and re-evaporation (blue); surface evaporation and boundary-layer dynamics (cyan). We used a 5 day filter to focus on seasonal and synoptic variations.

ACPD
14, 4457–4503, 2014

CC BY

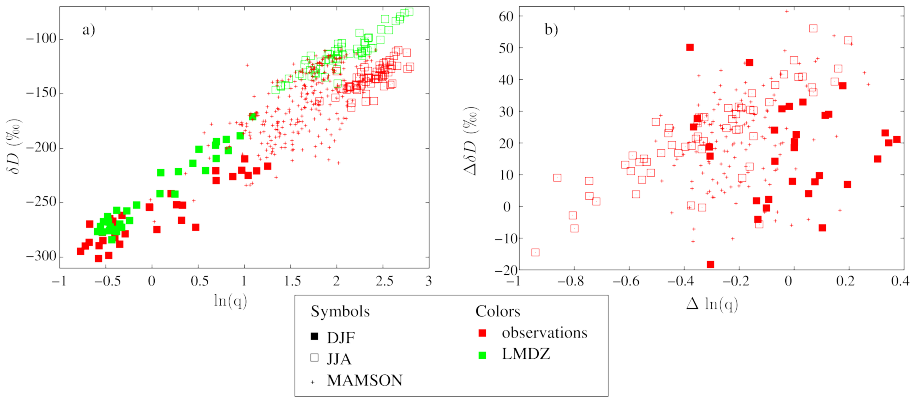

Fig. 12. (a) δD as a function of ln(q), in the observed data (red) and in the model (green). **(b)** $\Delta\delta$D as a function of Δln(q). Δ refers to the model-data difference. Symbols refer to the season: December-January-February (filled squares), June-July-August (empty squares) and March-April-May-September-October-November (crosses).

ACPD
14, 4457–4503, 2014